molecules

MDPI

Article

Heptanuclear Silver Hydride Clusters as Catalytic Precursors for the Reduction of 4-Nitrophenol

Tunde L. Yusuf [1], Segun A. Ogundare [1,2], Michael N. Pillay [1] and Werner E. van Zyl [1,*]

[1] School of Chemistry and Physics, Westville Campus, University of KwaZulu-Natal, Chiltern Hills, Durban 4000, South Africa
[2] Department of Chemical Sciences, Olabisi Onabanjo University, Ago-Iwoye 120107, Nigeria
* Correspondence: vanzylw@ukzn.ac.za

Abstract: We report on the design, synthesis, and characterization of the first silver hydride clusters solely protected and stabilized by dithiophosphonate ligands and their application for the in situ generation of silver nanoparticles towards the catalytic reduction of 4-nitrophenol in an aqueous system. The synthesis of the silver monohydride cluster involves the incorporation of an interstitial hydride using sodium borohydride. Poly-nuclear magnetic resonance and mass spectrometry were used to establish the structural properties. The structural properties were then confirmed with a single-crystal X-ray diffraction analysis, which showed a distorted tetracapped tetrahedron core with one hydride ion encapsulated within the core of the silver framework. Additionally, the synthesized heptanuclear silver hydride was utilized as a precursor for the in situ generation of silver nanoparticles, which simultaneously catalyzed the reduction of 4-nitrophenol. The mechanism of the catalytic activity was investigated by first synthesizing AgNPs, which was subsequently used as a catalyst. The kinetic study showed that the pseudo-first constant obtained using the cluster (2.43×10^{-2} s^{-1}) was higher than that obtained using the synthesized AgNPs (2.43×10^{-2} s^{-1}). This indicated that the silver monohydride cluster was more active owing to the release of the encapsulated hydride ion and greater reaction surface prior to aggregation.

Keywords: silver; cluster; hydride; catalysis; dithiophosphonate; complexes; nanoparticles

check for updates

Citation: Yusuf, T.L.; Ogundare, S.A.; Pillay, M.N.; van Zyl, W.E. Heptanuclear Silver Hydride Clusters as Catalytic Precursors for the Reduction of 4-Nitrophenol. *Molecules* **2022**, *27*, 5223. https://doi.org/10.3390/molecules27165223

Academic Editor: Boggavarapu Kiran

Received: 29 June 2022
Accepted: 11 August 2022
Published: 16 August 2022

Publisher's Note: MDPI stays neutral with regard to jurisdictional claims in published maps and institutional affiliations.

Copyright: © 2022 by the authors. Licensee MDPI, Basel, Switzerland. This article is an open access article distributed under the terms and conditions of the Creative Commons Attribution (CC BY) license (https://creativecommons.org/licenses/by/4.0/).

1. Introduction

Since the synthesis of the first binary transition metal hydride reported by Wurtz in 1844 [1], transition metal hydrides have been topical research avenues owing to their interesting structural and bonding properties as well as their application in hydrogen storage technology and catalysis [2–12]. Metal hydrides have been proposed to be a key intermediate in many catalytic processes [13–16]. For example, the dehydrogenation of alcohol to a ketone catalyzed by silver clusters supported on Al_2O_3 is believed to proceed via Ag–H intermediates [17,18]. Silver clusters supported on alumina have also been applied as a heterogeneous catalyst in the direct *N*-alkylation of anilines with benzyl alcohol [19], selective reduction of NO_x for automobile application [20–22], oxidant free C–H reduction of alcohol, C–C cross-coupling of secondary alcohols with primary alcohols [17,18] and amide synthesis from direct addition of alcohol with silver hydride proposed to be a key intermediate in the catalytic systems. Despite these remarkable and unique properties of transition metal hydrides, the structural aspect of this chemistry has often been hindered by instability and difficulty in isolating suitable crystals for X-ray diffraction studies. A remarkable number of copper hydride clusters of high nuclearity have been synthesized via a ligand-protected route, including $Cu_8(H)$, $Cu_{20}(H)_{11}$ [23,24], $Cu_{28}(H)_{15}$ [25], and $Cu_{32}(H)_{20}$ [26,27]. The synthesis is achieved via the chemical addition of ligand and copper salt in the presence of a hydride source such as borohydride (BH_4^-).

There is, however, a paucity of information available on these metal hydride clusters due to their instability in air. Although mixed silver-transition metal clusters such as

[Ru–H–Ag] [28], [Mo–H–Ag] [29], [Mn–H–Ag] [30], [Ir–H–Ag] [31], [Pt–H–Ag] [32] are well known, the ligand protected synthetic method has yielded stable and structurally characterized silver cluster such as $Ag_6(H)_4$ [33], $Ag_7(H)$ [34] and $Ag_8(H)$. As ligands, dichalcogenides have become an important class for stabilizing metal clusters. Liu and co-workers have reported the synthesis of Ag clusters capped by dithiophosphate and dithiocarbamate ligands [34]. To date, there is no report of dithiophosphonate solely capped large clusters, presumably owing to their steric demand and asymmetrical nature of the ligand, preventing efficient crystal packing. Rothenberger and co-workers reported the synthesis of Ag_{28} stabilized by dithiophosphonate but employed triphenylphosphine as a secondary ligand to aid the crystallization of silver clusters capped by dithiophosphonates [35].

There is, however, still a dearth of information to be unraveled on the synthesis, structural characterization, and catalytic properties of silver hydride clusters solely capped by dithiophosphonate ligands. In continuing our work on metal complexes and clusters of dithiophosphonates [36–39], we report the synthesis of four new Ag_7H clusters protected by dithiophosphonate ligands and demonstrate their application as precursors for in situ synthesis of silver nanoparticles as catalysts in the chemical reduction of 4-nitrophenol (4-NP) to 4-aminophenol (4-AP).

The reduction of 4-NP to 4-AP by borohydride is considered a reliable reaction model for assessing the catalytic properties of nanostructures [40,41]. The US Environmental Protection Agency (EPA) has listed 4-nitrophenol (4-NP) as one of the 129 organic chemicals which are carcinogenic and harmful to humans, animals, and plants due to their persistence, stability and resistance to biodegradation [42]. 4-NP is abundant in industrial effluents and soil because of its importance in producing dye, pharmaceuticals, herbicides, and insecticides [42–44]. Therefore, the reduction of 4-NP to 4-AP is a more sustainable solution since 4-AP is environmentally benign and an essential precursor in many organic syntheses.

Noble metal nanoparticles have been extensively researched as catalysts for the reduction of 4-NP [45], and there are several reports on AgNPs as an efficient catalyst for the reduction of 4-NP to 4-AP [46,47]. Still, there are only a few reports of silver clusters as a catalyst for this reduction reaction. This is the first structurally characterized silver hydride cluster utilized as a catalyst in the reduction of 4-NP to 4-AP.

2. Results and Discussion

2.1. Synthesis of the Silver Clusters

Clusters **1–4** were synthesized in good yield (>70%) from the reaction between $[Ag(CH_3CN)_4]PF_6$, dithiophosphonate (DTP) ligand, and sodium borohydride in a ratio of 7:6:1 under a nitrogen atmosphere for 3 h in THF (Scheme 1). The DTP ligands were derivatized using various alcohol; we observed that clusters from MeOH, EtOH, were unstable at room temperature and could not be characterized further. The clusters were isolated as a yellow powder, soluble in toluene, DCM, chloroform, acetone, and benzene and insoluble in hexane, water, and alcohol. All clusters were characterized by elemental analysis, electrospray ionization mass spectrometry, multinuclear NMR and UV-Visible spectroscopy. The structure of **1** was determined by single-crystal X-ray diffraction, whilst data was also collected for **3** and **4**, but unfortunately was of poor quality (see Supporting Information). The synthesis of the silver cluster includes the use of sodium borohydride, allowing for the possibility of an interstitial hydride encapsulated within the cluster. To explore this, the synthesis of **1** and **2** were repeated using $NaBD_4$ instead of $NaBH_4$ as a hydride source; ($\mathbf{1_D}$ and $\mathbf{2_D}$) and investigated using the ^{1}H-NMR and high-resolution mass spectrometry. The hydride provided by BH_4^- acts as the anionic template to yield $[Ag_7(H)L_6]$.

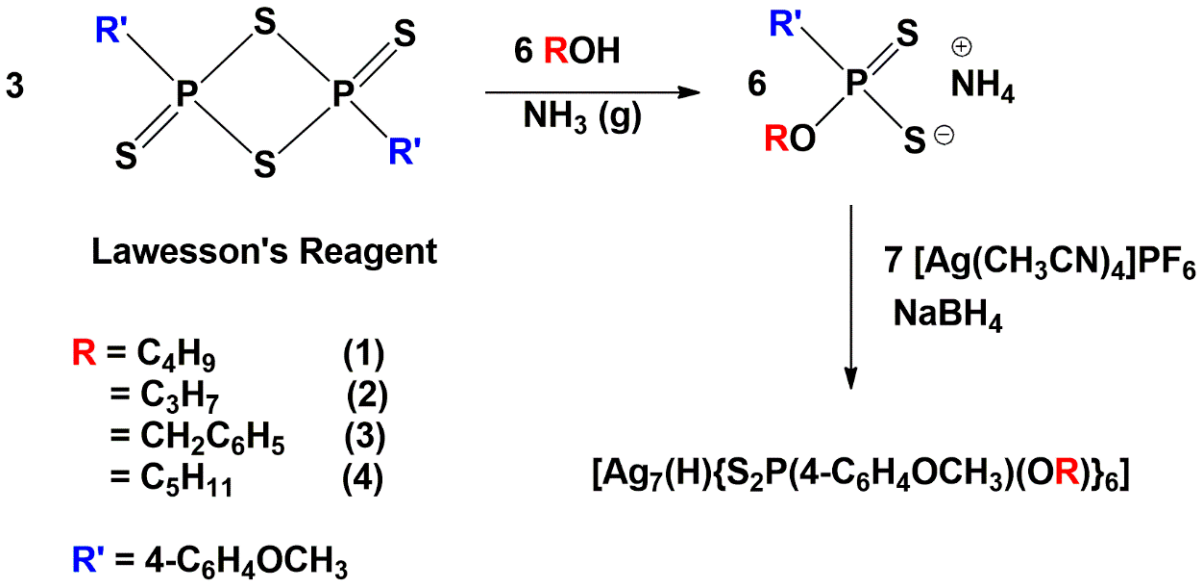

Scheme 1. The reaction scheme for the synthesis of the silver monohydride clusters.

2.2. Nuclear Magnetic Resonance (NMR) Spectroscopy

The ^{1}H-NMR for clusters **1**–**4** showed all the ligand functionalities. An additional quartet peak was observed in the spectra of **1** and **2** at 4.11 and 3.77 ppm (Figure S1a,b, Supplementary Materials), respectively, which integrates as 1 relative to the 18 methoxy protons on the anisole ring of the six capping DTP ligands which suggested the presence of an interstitial hydride within the cluster. To further confirm this, the synthesis of **1** and **2** were repeated using deuterated sodium borohydride ($NaBD_4$) as a hydride source instead of $NaBH_4$; $\mathbf{1_D}$ and $\mathbf{2_D}$. The disappearance of the peaks observed at 4.11 and 3.43 ppm confirmed the presence of an interstitial hydride within the heptanuclear core. The ^{1}H-NMR of **3** and **4** also displayed all the ligand functionalities and additional broad peaks at 4.71 and 4.01 ppm, respectively, and integrated to 1 relative to 18 methoxy protons of the six anisole rings. Only one singlet peak was observed for all clusters in the solution ^{31}P-NMR spectra, which appeared at 108, 107, 101 and 103 ppm for **1**, **2**, **3** and **4**, respectively. Possible peaks that could be associated with precursor PF_6^- counter anion was completely absent, as observed in the ^{31}P-NMR spectra of the clusters (Figures S2 and S3, Supplementary Materials). The singlet peak found in the ^{31}P-NMR spectra suggested that all the phosphorus atoms were in a chemically and magnetically equivalent environment. The possibility of an encapsulated hydride in an $M_7(H)L_6$ and $M_8(H)L_6$ (L = dithiocarbamate or dithiophosphate) has been proven unequivocally by Liu and co-workers by neutron diffraction analysis in $Cu_7(H)$ and NMR (^{2}H-NMR, ^{109}Ag) [48]. In the M_7 systems, the hydride (H^-) is required to balance the charge in an otherwise stable and overall neutral cluster containing seven mono-cation metals and six mono-anionic ligands. This work employed the use of unsymmetrical dithiophosphonate ligands (allowing for the potential formation of isomers) instead of symmetrical dithiocarbamate and dithiophosphate used by Liu and co-workers.

2.3. Mass Spectrometry

The chemical composition of **1**–**4** was further confirmed by positive ion electrospray ionization mass spectrometry (ESI-MS). The molecular ion peaks for clusters **1** and $\mathbf{1_D}$ expected at 2408.17 and 2409.18, respectively, were not observed. However, the HRMS spectra (Figures S4 and S5, Supplementary Materials) of clusters **1** and $\mathbf{1_D}$ showed adduct peaks at m/z: 2516.425 (calcd 2516.037) and 2517.447 (calcd 2517.043), which were equivalent to the entire molecular species with an additional silver ion to form an adduct ion corresponding to a mono-charged ion of $[Ag_7(H)L_6 + (Ag)]^+$ and $[Ag_7(D)L_6 + (Ag)]^+$, respectively. This is consistent with previously reported $Ag_7(H)L_6$ [34] and $Cu_7(H)(dtc)_6$

(dtc = dithiocarbamate) [48] clusters, which indicates that the neutral Ag_7 clusters bind strongly with Ag^+ under ESI gas-phase conditions. Positive mode ESI-MS was also used to determine the chemical composition of **2**. The peak at *m*/*z*: 2432.30 in the HRMS spectrum (Figure S6, Supplementary Materials) of cluster **2** corresponded to $[Ag_7(H)L_6 + (Ag)]^+$. Similarly, its low-resolution mass spectrum (Figure S7, Supplementary Materials) also displayed fragments at *m*/*z*: 2322.40, 1952.50, 1584.58, 1214.85, and 846.73 corresponding to $Ag_7(H)L_6$, $Ag_6(H)L_5$, $Ag_5(H)L_4$, $Ag_4(H)L_3$, $Ag_3(H)L_2$, respectively. The HRMS spectrum (Figure S8, Supplementary Materials) of cluster **4** also showed a molecular ion peak at 2600.53 (calcd 2600.20) corresponding to $[Ag_7(H)L_6 + Ag]^+$. However, for cluster **3**, the molecular ion peak expected at 2612.26 was not observed. Instead, an M^{2+} peak at 1468.00 (calcd 1468.00) corresponding to $[Ag_7(H)L_6 + Ag]^{2+}$ was observed in the mass spectrum (Figure S9, Supplementary Materials).

2.4. X-ray Crystallography

Cluster **1**—The crystal structure of **1** revealed that the heptanuclear neutral silver cluster crystalized in a triclinic P (−1) space group with the seven silver atoms disordered in sixteen positions. The asymmetric unit showed two distorted tetrahedrons disordered over each other, as shown in Figure 1. The entire silver framework formed a cage with an encapsulated hydride within the heptanuclear cage. The occupancy for each of the silver atoms in one of the tetrahedrons in the asymmetric unit was fixed at 50% ($0.5 \times 8 = 4$), accounting for four of the silver atoms in the molecule. To account for the remaining three silver atoms in eight positions, two Ag units were fixed at 50%, two at 43%, two at 44%, and two at 13%. The silver framework adopts a distorted tetracapped tetrahedron core with one hydride ion encapsulated within the core. The Ag_7 core is surrounded by 12 S atoms from 6 bridging dithiophosphonate ligands in a distorted icosahedral cage. A similar disorder is observed on related dithio-based ligands in Ag_7 [35], Cu_7 [48], Ag_8 [49] clusters. The vertex silver atoms in the inner tetrahedron consisted of Ag_1, Ag_3 Ag_5 and Ag_7 (abbreviated as Ag_{cap}) and capped by Ag_2, Ag_4, Ag_8, and Ag_6 (abbreviated as Ag_v). The distances Ag_v–Ag_v fall in the range 3.0522(17)–3.2201(17) Å, while those of Ag_v–Ag_{cap} fall in the range 2.9763(19)–3.3019(18) Å. The dithiophosphonate ligands are coordinated in a tetraconnective tetrametallic (μ_2, μ_2) mode. This presents the first report of dithiophosphonate ligand coordinated to silver atoms in this coordination pattern (μ_2, μ_2). For the Ag–S distances, the Ag_v–S ranges from 2.564–2.739Å, and the Ag_{cap}–S distances are within the range of 2.342(3)–2.564(3) Å. The distances for Ag_v–S are longer than those of Ag_{cap}–S, which are normal and well within the expected range. The interstitial hydride is located on a crystallographic center of inversion. The distances between the encapsulated hydride and the silver atoms are in the range of 1.987–2.061 Å. The Ag–H distances are comparable to those of Ag_7 and Ag_8 reported [34,49,50]. Furthermore, four anisole rings of the six ligands are disordered over two positions and are fixed at 50% occupancy each.

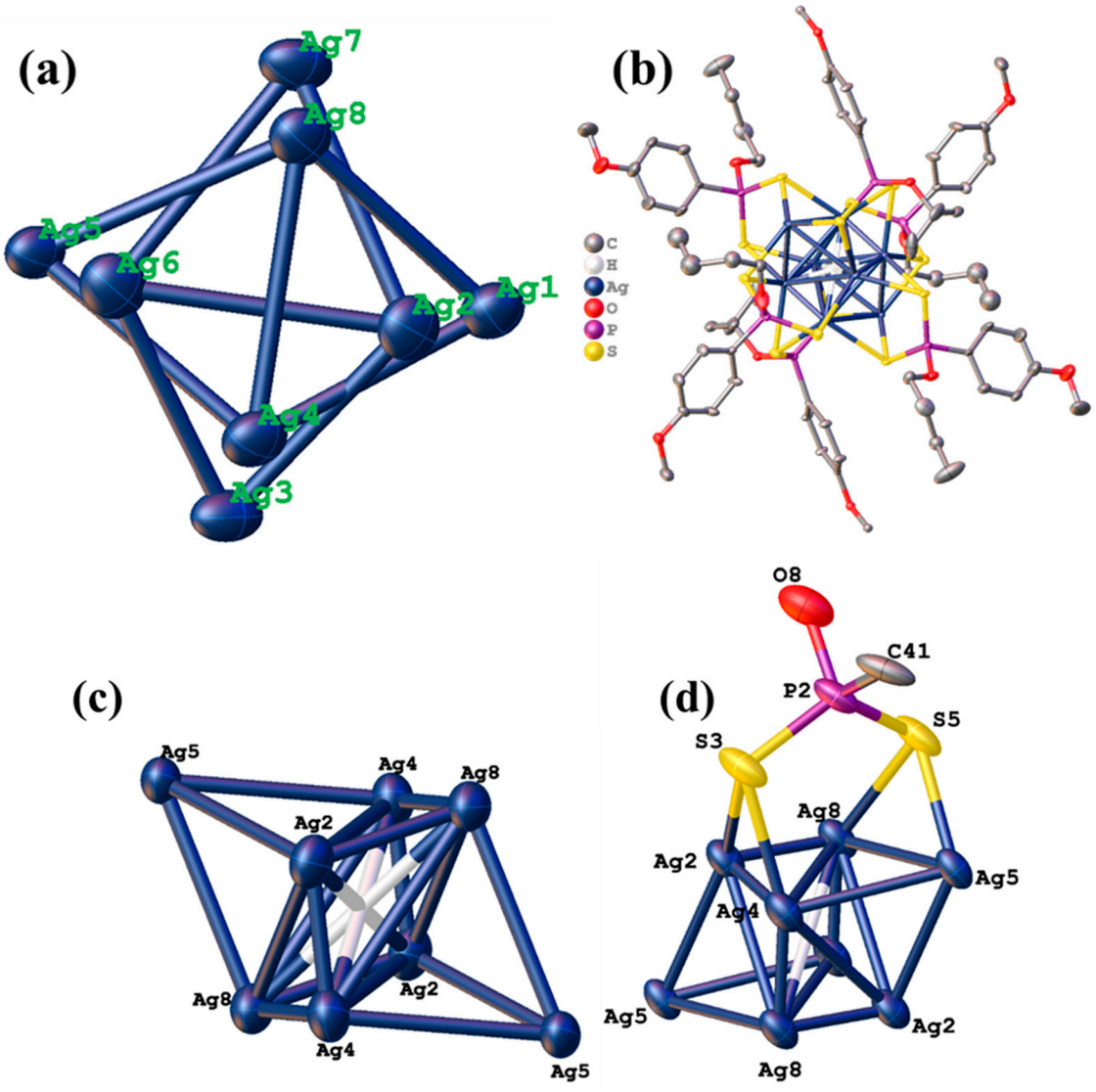

Figure 1. (**a**) Molecular structure of cluster **1**. H-atoms omitted for clarity except for the interstitial hydride. (**b**) Molecular representation of the asymmetric unit for **1** showing only the silver atoms. (**c**) Ag_7H core structural representation. (**d**) Coordination motif of DTP ligand to the silver core.

3. In Situ Production of Silver Nanoparticle and Reduction of 4-Nitrophenol

Silver nanoparticles have been reported to show outstanding catalytic activity and selectivity in the reduction of 4-NP [51]. The catalytic efficiency of the Ag_7 cluster was examined via the reduction of 4-NP to 4-AP. To access the role of the interstitial hydride within the Ag_7 cluster, the catalytic properties of the silver precursor $[Ag(CH_3CN)_4]PF_6$ were also investigated. The reaction was carried out in a one-step method, and the change in absorbance was monitored over time using UV-visible spectroscopy at one-minute intervals. Cluster **1** was added to a mixture of 4-NP and $NaBH_4$ in a 4 mL cuvette. The catalytic property of the cluster was examined by monitoring the spectral changes in the absorption spectrum of 4-(hydroxyamino)phenol. The spectroscopic monitoring showed a rapid reduction of 4-NP. It was established that the reduction reaction of 4-NP to 4-AP proceeds through an intermediate 4-(hydroxyamino)phenol (Scheme 2). Upon the addition of $NaBH_4$ to 4-NP, the band of 4-NP immediately shifted from 317 nm to 400 nm, which indicated the formation of 4-nitrophenolate, which has been established as the first stable intermediate form. In the absence of a catalyst, the absorbance of the intermediate remained unchanged after several hours, which suggested that the reaction did not proceed in the absence of a catalyst. The procedure was repeated with the addition of precursor $[Ag(CH_3CN)_4]PF_6$ as

a catalyst, but no significant change was observed in the absorption maxima after several hours, which suggested that the silver starting material does not catalyze the reduction of 4-NP. However, when cluster **1** was introduced as a catalyst, the band at 400 nm started to decrease with time, and a corresponding new band appeared at 300 nm, which indicated the formation 4-AP (Figure 2a). It was observed that a simultaneous reduction of silver ions in cluster **1** used as a catalyst occurred alongside the reduction of 4-NP, which indicated that the catalytic activity of cluster **1** proceeded via the in situ generation of AgNPs. This was further investigated by first chemically reducing cluster **1** using $NaBH_4$; the AgNPs isolated were characterized and subsequently used as a catalyst following a similar procedure. The result of the study showed that the derived AgNPs from cluster **1** were equally active as a catalyst for the complete reduction of 4-NP.

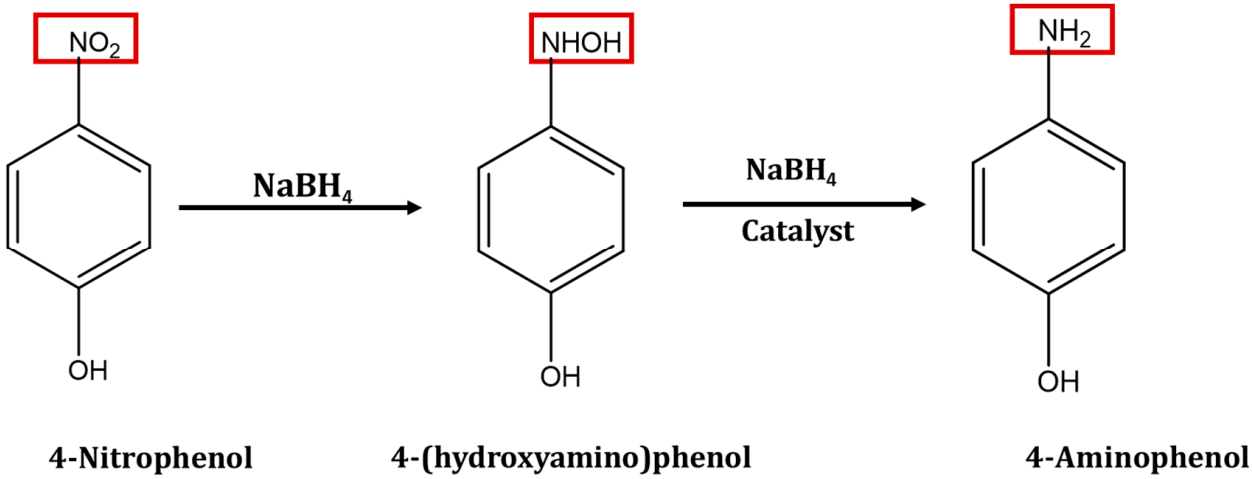

Scheme 2. Catalytic reduction of 4-NP to 4-AP.

When cluster **1** was used as a catalyst, the catalytic reduction of 4-NP was driven to completion in about 3 min, while with AgNPs, the reduction of the reaction of 4-NP took about 4 min. The observed difference in time of completion indicated that the in situ generation of AgNPs (as opposed to adding previously isolated AgNPs) provided improved catalytic efficiency, which suggests greater activity resulting from the higher surface area of the in situ generated AgNPs prior to aggregation and also the release of the active participation of the interstitial hydride ion within cluster **1**. Since excess $NaBH_4$ was used in comparison with 4-NP, the reaction is proposed to be a pseudo-first-order reaction. The kinetics of the reaction may be described as $\ln(C/C_o) = -kt$, where k is the first-order rate constant (min^{-1}), t is reaction time; C is the concentration of 4-NP at time t, and C_o is a concentration of 4-NP at time 0. The rate constant k of cluster **1** was calculated to be 2.43×10^{-2} s^{-1} with a correlation coefficient of 0.9982, while for the derived AgNPs, the rate constant k was calculated to be 1.02×10^{-2} s^{-1} with a correlation coefficient of 0.9909. It has been previously shown that the presence of highly reactive silver hydride Ag–H, within the cluster and in the presence of $NaBH_4$ is considered a key mediator to the catalytic performance of the silver clusters for the reduction of 4-NP by aiding the transfer of hydrogen in the system [52].

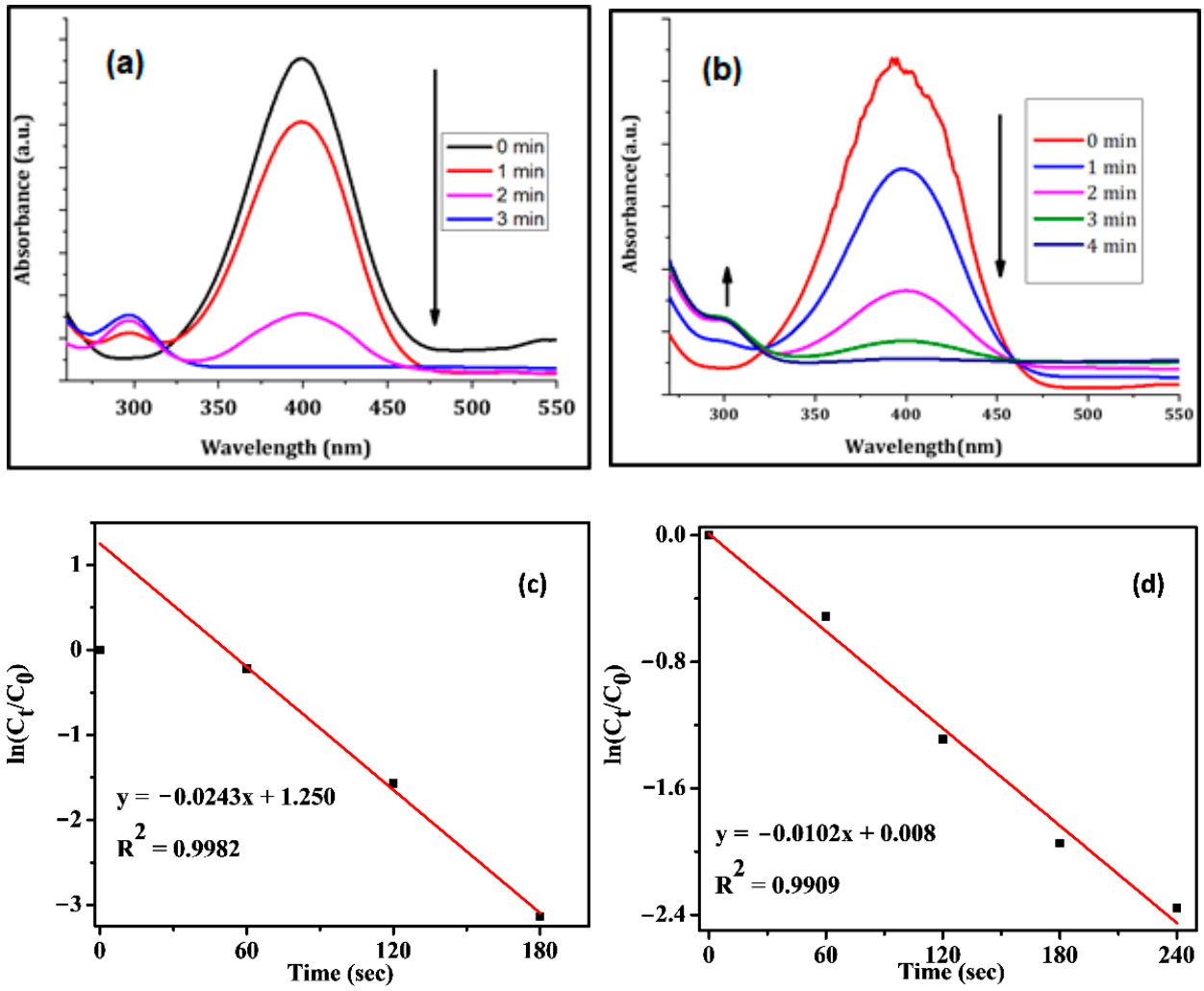

Figure 2. UV-vis spectra showing the successive reduction of 4-NP to 4-AP in the presence of (**a**) cluster **1** (corresponding kinetic plots (**c**)) and (**b**) the derived AgNPs at room temperature (corresponding kinetic plots (**d**)).

Under similar conditions, the catalytic properties of cluster **1** and AgNPs are comparable with the reaction time of 3 min and 4 min, respectively, and corresponding percentage reduction of 96% and 92%, respectively. Cluster **1** transformed to AgNPs after the first cycle. This prompted the investigation and characterization of the AgNPs, which revealed that the AgNPs were generated in situ and remained stable and reusable after recovery and washing with water via centrifugation. The percentage reduction was ~90% after 5 cycles (Figure S12, Supplementary Materials). The catalytic activity of silver nanoparticles is attributed to the presence of readily available surface electrons on the nanoparticles. The activity of cluster **1** is due to the presence of very reactive silver hydride, and the subsequent rich electrons available at the surface of the in situ generated AgNPs.

4. Properties of Cluster 1 and the Synthesized Silver Nanoparticles

The properties were elucidated using high-resolution transmission electron microscopy (HRTEM), scanning electron microscopy (SEM), Fourier-transform infrared (FT-IR) and UV-visible (UV-vis) spectroscopies.

The electronic spectra of cluster **1** and the AgNPs recorded in dichloromethane and water, respectively, showed peaks at 340 nm (cluster **1**) and 420 nm (AgNPs) (Figure 3a). The absorption peak of the AgNPs indicated the localized surface plasmon resonance characteristics of AgNPs. Unlike the synthesized AgNPs, cluster **1** showed absorption

maxima at a shorter wavelength in the ultraviolet region, which suggested a metal-to-ligand charge transfer (MLCT).

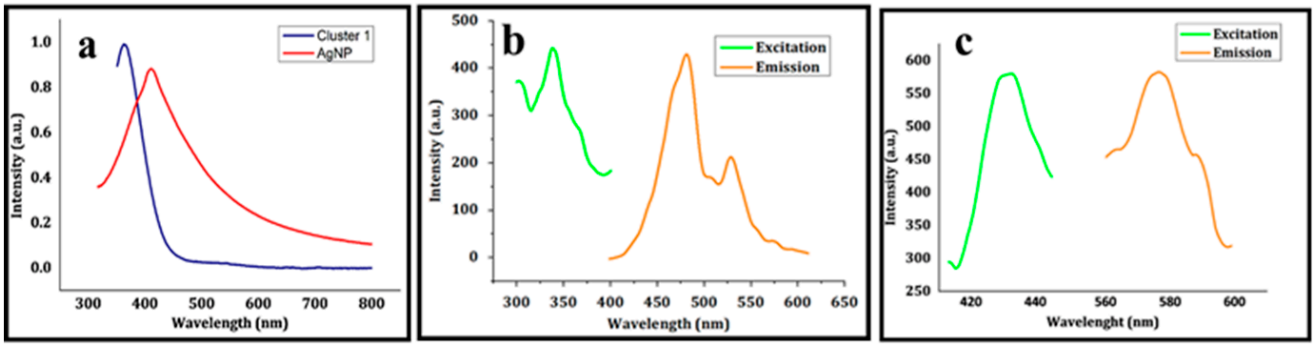

Figure 3. (**a**) Electronic absorption spectrum of cluster **1** (Blue) and AgNPs (red). (**b**) Excitation spectrum of AgNPs (green) and emission spectrum (orange). (**c**) Excitation spectrum of cluster **1** (green) and emission spectrum (orange).

Upon excitation at 430 nm, cluster **1** and the AgNPs showed orange emissions at room temperature at 482 nm (cluster **1**) (Figure 3c) and 560 nm with a shoulder at 579 nm (AgNPs) (Figure 3b). The precise mechanism for the silver nanoparticle fluorescence is unclear, but the polycrystalline structures of silver nanoparticles with numerous ultra-small domains and the particle-supported ultra-small silver nanoclusters could be the possible reasons for the observed luminescence. Moreover, the shoulder observed at 579 nm could be attributed to the presence of silver nanoclusters aggregates with different numbers of atoms.

The SEM micrograph (Figure 4a) revealed that the nanoparticles formed were polydispersed. Close observation showed that the nanoparticles adopted a spherical morphology with few having irregular shapes. The morphology and particle size investigated using HRTEM (Figure 4b) further confirmed the spherical and non-aggregated nature of the nanoparticles as observed in the SEM micrographs. The histogram of the nanoparticle size distribution obtained from the analysis of the HRTEM micrograph of the synthesized AgNPs (Figure 4c) indicated that the sizes of the nanoparticles range from 4–12 nm with an average of 6 nm.

Energy dispersion X-ray analysis determined the elemental constituents of the synthesized AgNPs. The EDX spectrum (Figure 4d) showed silver as the dominant species with a highly intense peak at a binding energy of 3 keV characteristics of silver. It also showed the presence of phosphorus and sulfur, which indicated the presence of the ligand and suggested that the dithiophosphonate ligand provided a stabilizing effect for the AgNPs. The FTIR analysis further supported this. By comparing the IR spectrum of AgNPs with those of cluster **1** and the ligand (Figure S10, Supplementary Materials), the major vibrational frequencies of the ligand were also observed in the clusters and in the synthesized nanoparticles, which indicated the capacity of the dithiophosphonate ligand to act as a capping agent for the cluster as well as a stabilizing agent to prevent excessive aggregation in the subsequently in situ generated silver nanoparticles.

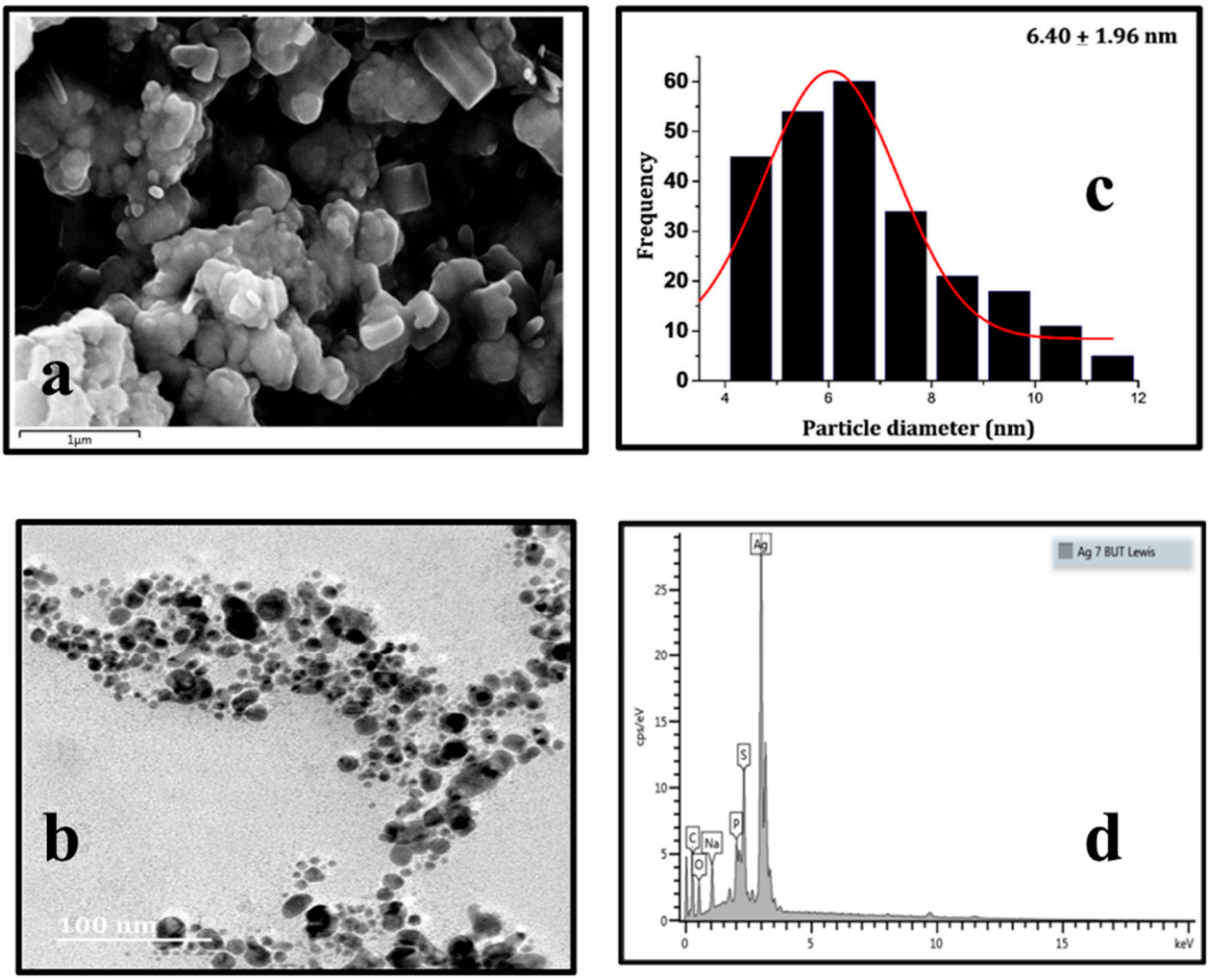

Figure 4. (**a**) SEM micrographs of AgNPs. (**b**) TEM micrographs of AgNPs. (**c**) Particle size distribution of AgNPs. (**d**) EDX spectrum of AgNPs.

5. Materials and Methods

5.1. General Procedures and Instrumentation

All reactions were performed using standard Schleck techniques under a nitrogen atmosphere. All chemicals were purchased from commercial sources and are of analytical grade. THF and DCM were dried using PURE-SOLV solvent purification system, (Innovative Technology, Amesbury, MA, USA, now known as inert, inertcorp.com). $[Ag(CH_3CN)_4]PF_6$ [53] and $NH_4[S_2P(4\text{-}C_6H_4OMe)(OR)]$ derivatives [54,55] were prepared following literature procedures. NMR spectra were recorded on a Bruker AV-400 instrument (Billerica, MA, USA) operating at 400MHz. The ^1H and ^{31}P-NMR spectra were recorded at 162 MHz. For the ^1H-NMR, the residual solvent proton was used as a reference (δ, ppm, $CDCl_3$, 7.26). For ^{31}P-NMR, H_3PO_4 (85%) was used as an external reference. The melting point was determined on an Electrothermal 9100 melting point apparatus (Stone, UK) and was uncorrected. The electronic absorption spectra were recorded on a Shimadzu UV-3600 UV-VIS-NIR spectrophotometer (Kyoto, Japan) using quartz cuvettes with a path length of 1 cm in the 200–400 nm for UV and 400–900 nm visible regions. The emission spectra were recorded on Perkin Elmer LS 55 fluorescence spectrometer (Waltham, MA, USA). Electrospray ionization mass spectrum (ESI-MS) for cluster **1** was recorded on Waters Micromass LCT Premier TOF-MS (Milford, MA, USA).

5.2. Synthesis of Silver Clusters

5.2.1. Synthesis of cluster **1** ($[Ag_7(H)\{(S_2P(4\text{-}C_6H_4OMe)(OC_4H_9)\}_6]$)

In an oven-dried Schlenk flask $[NH_4]\{S_2P(4\text{-}C_6H_4OMe)(OC_4H_9)\}$ (251 mg, 0.857 mmol) and $NaBH_4$ (5.4 mg, 0.142 mmol) were suspended in 15 mL of anhydrous THF. Subsequently, $[Ag(CH_3CN)_4PF_6]$ (417 mg, 1.000 mmol) was added to the reaction mixture and stirred at 0 °C for 3 h. The resulting yellow solution was pumped down under reduced pressure. The residue was dissolved in DCM and washed with deionized water (3 × 15 mL). The DCM fraction was filtered through Celite and dried under reduced pressure. The resulting yellow residue was added to hexane and kept in a refrigerator for several hours. The air and moisture stable yellow powder was obtained by filtration. Yield: 270 mg (92%). Melting point: 112 °C. Anal. Calculated for $C_{66}H_{97}Ag_7O_{12}P_6S_{12}$: C, 32.92; H, 4.06; S, 15.98% Found: C, 32.39, H, 4.25. S, 16.22%. ^{1}H-NMR (400 MHz, Chloroform-*d*) δ 8.00 (dd, *J* = 13.7, 8.5 Hz, 12H, Ar–H), 6.93 (dd, *J* = 8.8, 3.1 Hz, 12H, Ar–H), 4.11 (q, *J* = 6.8 Hz, 1H, Ag–H), 4.02 (t, *J* = 7.1 Hz, 12H, OCH_2), 3.85 (s, 18H, OCH_3), 1.67 (dd, *J* = 8.5, 6.3 Hz, 12H, CH_2), 1.40 (h, *J* = 7.2 Hz, 12H, CH_2), 0.91 (t, *J* = 7.3 Hz, 18H, CH_3). ^{31}P-NMR (162 MHz, $CDCl_3$) 108.28 (6P, s). ESI-MS (*m*/*z*) $[M + Ag]^+$ 2516.00 (calcd 2516.40). UV-VIS [λ_{max} (ε)] 367 nm, 19, 600 M^{-1} cm^{-1}. Single-crystal suitable for X-ray analysis was obtained as a colourless rod from a mixture of acetone and hexane.

5.2.2. Synthesis of Cluster $\mathbf{1}_D$ ($[Ag_7(D)\{(S_2P(4\text{-}C_6H_4OMe)(OC_4H_9)\}_6]$)

Cluster $\mathbf{1_D}$ was synthesized in 96% yield (280 mg, based on Ag) by following the aforementioned method using $NaBD_4$ as a deuteride source instead of $NaBH_4$ as a hydride source. Mp: 111 °C, Anal. Calcd for $C_{66}H_{96}DAg_7O_{12}P_6S_{12}$: C, 32.92, H, 4.10 S, 15.97 Found: C, 32.40, H, 4.29 S, 16.22. ^{1}H-NMR (400 MHz, Chloroform-*d*) δ 8.01 (dd, *J* = 13.7, 8.5 Hz, 12H, Ar–H), 6.95 (dd, *J* = 8.8, 3.1 Hz, 12H, Ar-H), 4.05 (q, *J* = 7.1 Hz, 12H, OCH_2), 3.85 (s, 18H, OCH_3), 1.68 (dd, *J* = 8.5, 6.3 Hz, 12H, CH_2), 1.43 (h, *J* = 7.2 Hz, 12H, CH_2), 0.92 (t, *J* = 7.3 Hz, 18H, CH_3). HR-ESI-MS (*m*/*z*) $[M + Ag]^+$ 2517.00 (calcd 2517.45).

5.2.3. Synthesis of Cluster **2** ($[Ag_7(H)\{S_2P(4\text{-}C_6H_4OMe)(OC_3H_7)\}_6]$)

Cluster **2** was prepared in a similar manner to cluster **1**. Yield: 125 mg (90%, based on Ag) Mp: 108 °C, Anal. Calcd for $C_{60}H_{85}Ag_7O_{12}P_6S_{12}$: C, 31.01; H, 3.69; S, 16.55. Found: C, 30.80; H, 3.83; S, 16.97. ^{1}H-NMR (400 MHz, Chloroform-*d*) δ 7.91 (dd, *J* = 13.8, 8.4 Hz, 12H, Ar–H), 6.85 (dd, *J* = 7.8 Hz, 12H, Ar–H), 3.90 (t, *J* = 9.7 Hz, 12H, OCH_2), 3.77 (s, 18H, OCH_3), 3.77 (q, *J* = 2.6, 2.0 Hz, 1H, Ag–H), 1.66–1.61 (m, 12H, CH_2), 0.86 (t, *J* = 7.4 Hz, 18H, CH_3). ^{31}P-NMR (162 MHz, $CDCl_3$) 108.28 (6P, s). ESI-MS (*m*/*z*) $[M + Ag]^+$ 2432.35 (calcd 2432.33).

5.2.4. Synthesis of Cluster $\mathbf{2}_D$ ($[Ag_7(D)\ \{S_2P(4\text{-}C_6H_4OMe)(OC_3H_7)\}_6]$)

Cluster $\mathbf{2_D}$ was obtained in 90% yield (0.20 g, based on Ag) by following the aforementioned method using $NaBD_4$ as a deuteride source instead of $NaBH_4$ as a hydride source. Mp: 110 °C, Anal. Calcd for $C_{60}H_{84}DAg_7O_{12}P_6S_{12}$. C, 31.00; H, 3.73; S, 16.55 Found: $C_{60}H_{84}DAg_7O_{12}P_6S_{12}$. C, 30.42; H, 3.80; S, 16.85 ^{1}H-NMR (400 MHz, Chloroform-d) δ 7.89 (dd, *J* = 13.8, 8.4 Hz, 12H, Ar–H), 6.84 (dd, *J* = 7.8 Hz, 12H, Ar–H), 3.90 (d, *J* = 9.7 Hz, 12H, OCH_2), 3.77 (s, 18H, OCH_3), 1.65 (m, 12H, CH_2),0.85 (t, *J* = 7.4 Hz, 18H, CH_3). ESI-MS (*m*/*z*) $[M + Ag]^+$ 2433.31 (calcd 2433,34).

5.2.5. Synthesis of Cluster **3** ($[Ag_7(H)\{S_2P(4\text{-}C_6H_4OMe)(OCH_2C_6H_5)\}_6]$)

Cluster **3** was prepared in a similar manner to **1**. Yield: 101 mg (56%) ^{1}H-NMR (400 MHz, Chloroform-*d*): δ (ppm), 8.02 (dd, *J* = 9.01, 12H, Ar–H), 7.39 (d, *J* = 8.10 Hz, 12H, Ar–H), 7.35 (d, *J* = 7.56 Hz, 12H, Ar–H), 6.95 (dd, *J* = 8.78, 12H, Ar–H), 5.29 (s, 12H, CH_2), 4.71 (bs, 1H, Ag–H), 3.85 (s, 18H, OCH_3), ^{31}P-NMR (162 MHz, $CDCl_3$) 101.68 (6P, s). ESI-MS (*m*/*z*) $[M + Ag]^{2+}$ 1467.92 (Calcd 1468.00). Single crystals for X-ray analysis were obtained as yellow blocks by vapour diffusion of hexane into a concentrated DCM solution.

5.2.6. Synthesis of Cluster **4** ($[Ag_7(H)\{S_2P(4\text{-}C_6H_4OMe)(OC_5H_{11})\}_6]$)

Cluster **4** was prepared by adopting a procedure similar to that of cluster **1**. Yield: 123 mg (76%). Melting point: 121 °C. ^{1}H-NMR (400 MHz, DMSO-d_6) δ 7.76 (dd, J = 13.6, 8.5 Hz, 12H, Ar–H), 7.09 (dd, J = 8.7, 3.2 Hz, 12H, Ar–H), 4.01 (bs, 1H, Ag–H) 4.46 (dp, J = 11.6, 5.8 Hz, 6H, OCH), 3.83 (s, 18H, OCH_3), 1.66 (dq, J = 9.2, 7.1 Hz, 24H, CH_2), 0.93 (t, J = 7.4 Hz, 36H, CH_3), HR-ESI-MS (m/z) $[M + Ag]^+$ 2600.5259 (calcd 2600.20). A single crystal for X-ray analysis was obtained as a colourless rod by slow evaporation from a mixture of benzene and hexane.

5.3. Characterization of AgNP

The morphology of the AgNPs was examined using electron microscopy. The high-resolution transmission electron microscopy (HRTEM) analysis was conducted on a JEOL 2100 (Tokyo, Japan) high-resolution transmission electron microscope. The scanning electron microscopy analysis was conducted on a Zeiss Ultra Plus field emission gun scanning electron microscope (FEG-SEM) equipped with an energy dispersive X-ray (EDX) detector (Jena, Germany). The HRTEM images of the AgNPs were obtained by using 5 µL of each sample deposited on a copper TEM grid. The particle size was obtained by measuring the diameters of 150 AgNPs in the HTEM micrographs using ImageJ 1.42 software (NIH, Bethesda, MD, USA), and the obtained data were processed on OriginPro 8 software (OriginLab Corporation, Northampton, MA, USA). Similarly, the SEM images were obtained by depositing a dried product of AgNPs samples on a conductive carbon tape stuck to aluminum stubs. To minimize charging, the sample was coated with gold with the aid of a sputter coater.

5.4. Catalytic Reduction of 4-NP by Cluster **1** *and AgNPs*

For the reduction of 4-NP, the procedure employed a standard catalytic test, as reported by Kästner et al. [46]. An aqueous solution of 4-NP (2 mL, 10^{-4} M) was mixed with a freshly prepared aqueous solution of $NaBH_4$ (1 mL, 10^{-4} M) in a quartz cell (1.0 cm path length and 4.5 mL volume). Cluster **1** (2.5 µL, 6 nmol) was dispersion in water and was added to the solution. The reduction was monitored at room temperature using a UV-vis spectrophotometer scanning over a range of 250–550 nm with a successive 1 min interval at room temperature. The apparent rate constant (Kapp) of the catalytic reaction was determined by measuring the absorbance at 400 nm. This procedure was repeated using AgNPs as a catalyst.

5.5. X-ray Crystallographic Determination

Experimental. The single crystals of **1**, **3**, **4** were selected and mounted on a MITIGEN holder in paratone oil on a Bruker SMART APEX2 area detector diffractometer (Billerica, MA, USA). During data collection, the crystal was kept at T = 100(2) K. Using Olex2, [56] the structure was solved with the SHELXS-2013 [57] structure solution program, using the direct solution method. The model was refined with SHELXL [58] using Least Squares minimization. All non-hydrogen atoms were refined anisotropically. Most hydrogen atom positions were calculated geometrically and refined using the riding model, but some hydrogen atoms were freely refined.

6. Conclusions

The study demonstrated the synthesis of new air and moisture stable Ag_7 clusters ligated by dithiophosphonate ligands and characterized by single-crystal XRD, NMR, UV-Vis and luminescence spectroscopy. The crystal structure revealed that the dithiophosphonate (DTP) ligands were coordinated in a tetra-connective tetra-metallic (μ_2, μ_2) mode representing the first of this binding mode for DTP ligands and the first high nuclearity silver cluster stabilized by this ligand type. Cluster **1**, in the presence of excess borohydride, yielded silver nanoparticles and simultaneous reduction of 4-NP to 4-AP. The obtained nanoparticles were characterized by TEM, SEM, UV-Vis and luminescence spectroscopy

which revealed that the AgNPs are monolithic and luminescent, with an average size diameter of 6.4 nm. To establish the mechanism behind the catalytic activity of cluster **1**, AgNPs were first synthesized from cluster **1** and subsequently applied as a catalyst for the reduction of 4-NP. The cluster showed an excellent ability to reduce 4-NP, and expectedly the AgNPs also showed an excellent ability under the same conditions. We concluded the size and dispersion of the AgNPs are key components to account for their activity. The mechanism of reduction of 4-NP using silver hydride cluster, however, is not fully understood, but it is believed that the presence of reactive Ag-H species makes the transfer of hydride ion to the intermediate (4-(hydroxyamino)phenol) possible.

Supplementary Materials: The following supporting information can be downloaded at: https://www.mdpi.com/article/10.3390/molecules27165223/s1, Figure S1: ^{1}H-NMR spectrum for cluster **1**; Figure S2: ^{31}P-NMR spectrum for cluster **1**; Figure S3: ^{31}P-NMR spectrum for cluster **2**; Figure S4: HRMS for cluster **1**; Figure S5: HRMS for cluster $\mathbf{1_D}$; Figure S6: HRMS for cluster **2**; Figure S7: HRMS for cluster $\mathbf{2_D}$; Figure S8: HRMS for cluster **4**; Figure S9: Mass spec of cluster **3**; Figure S10: Comparative FT-IR spectra of DTP, cluster **1** and AgNPs; Figure S11: Mapping of the constituent elements of AgNps; Figure S12: Percentage catalytic reduction achieved with the AgNPs over 5 cycles; Table S1: Selected crystallographic data for 1; Table S2: Fractional Atomic Coordinates (×104) and Equivalent Isotropic Displacement Parameters (Å2 × 103) for Cluster **1**; Table S3: Anisotropic Displacement Parameters (Å2 × 103) for Cluster **1**; Table S4: Bond Lengths for Cluster **1**; Table S5: Bond Angles for Cluster **1**; Table S6: Torsion Angles for Cluster **1**; Table S7: Hydrogen Atom Coordinates (Å × 104) and Isotropic Displacement Parameters (Å2 × 103) for Cluster **1**; Table S8: EDX elemental constituent of AgNPs.

Author Contributions: Conceptualization, W.E.v.Z. and T.LY.; methodology, T.L.Y. and S.A.O.; software, M.N.P. and T.L.Y.; validation, M.N.P.; formal analysis, T.L.Y. and S.A.O.; investigation, W.E.v.Z. and T.L.Y.; resources, W.E.v.Z.; writing—original draft preparation, T.L.Y.; writing—review and editing, T.L.Y., M.N.P. and S.A.O.; supervision, W.E.v.Z.; project administration, M.N.P. and S.A.O.; funding acquisition, W.E.v.Z. All authors have read and agreed to the published version of the manuscript.

Funding: The authors gratefully acknowledge research funds provided by the University of KwaZulu Natal and for the research supported in part by the National Research Foundation of South Africa (Grant Number: 132014), and the Eskom TESP program.

Institutional Review Board Statement: Not applicable.

Informed Consent Statement: Not applicable.

Data Availability Statement: CCDC numbers 1980078 contain the supplementary crystallographic data for this paper. These data can be obtained free of charge via www.ccdc.cam.ac.uk/data_request/CIF, (access on 15 July 2022) by emailing data_request@ccdc.cam.ac.uk, or by contacting The Cambridge Crystallographic Data Centre, 12 Union Road, Cambridge CB2 1EZ, UK; fax: +44-1223-336033. Crystallographic details.

Acknowledgments: We are grateful to the University of KwaZulu-Natal (UKZN) for providing the facility for this research.

Conflicts of Interest: The authors declare no conflict of interest.

Sample Availability: Samples are available from authors pending decomposition over time.

References

1. Wurtz, A. Sur l'hydrure de cuivre. *Ann. Chim.* **1844**, *11*, 250–252.
2. Kaesz, H.D.; Saillant, R.-B. Hydride complexes of the transition metals. *Chem. Rev.* **1972**, *72*, 231–281. [CrossRef]
3. Lin, Z.; Hall, M.B. Transition metal polyhydride complexes: A theoretical view. *Coord. Chem. Rev.* **1994**, *135*, 845–879. [CrossRef]
4. Pillay, M.N.; Van Zyl, W.E.; Liu, C.W. A construction guide for high-nuclearity (≥50 metal atoms) coinage metal clusters at nanoscale: Bridging molecular precise constructs with the bulk materials phase. *Nanoscale* **2020**, *12*, 24331–24348. [CrossRef]
5. Maseras, F.; Lledos, A.; Clot, E.; Eisenstein, O. Transition metal polyhydrides: From qualitative ideas to reliable computational studies. *Chem. Rev.* **2000**, *100*, 601–636. [CrossRef] [PubMed]
6. Hoskin, A.J.; Stephan, D.W. Early transition metal hydride complexes: Synthesis and reactivity. *Coord. Chem. Rev.* **2002**, *233*, 107–129. [CrossRef]

7. Morris, R.H. Dihydrogen, dihydride and in between: NMR and structural properties of iron group complexes. *Coord. Chem. Rev.* **2008**, *252*, 2381–2394. [CrossRef]
8. Van Zyl, W.E.; Liu, C.W. Interstitial hydrides in nanoclusters can reduce M(I) (M = Cu, Ag, Au) to M(0) and form stable superatoms. *Chem.–Eur. J.* **2022**, *28*, e202104241. [CrossRef]
9. Gloaguen, F.; Rauchfuss, T.B. Small molecule mimics of hydrogenases: Hydrides and redox. *Chem. Soc. Rev.* **2009**, *38*, 100–108. [CrossRef]
10. King, R. Structure and bonding in homoleptic transition metal hydride anions. *Coord. Chem. Rev.* **2000**, *200*, 813–829. [CrossRef]
11. Dhayal, R.S.; Van Zyl, W.E.; Liu, C.W. Copper hydride clusters in energy storage and conversion. *Dalton Trans.* **2019**, *48*, 3531–3538. [CrossRef] [PubMed]
12. Henderson, R.A. Metal hydride intermediates in hydrogenases and nitrogenases: Enzymological and model studies. In *Recent Advances in Hydride Chemistry*, 1st ed.; Peruzzini, M., Poli, R., Eds.; Elsevier: Amsterdam, The Netherland, 2001; pp. 463–505.
13. Angelici, R.J. Heterogeneous catalysis of the hydrodesulfurization of thiophenes in petroleum: An organometallic perspective of the mechanism. *Acc. Chem. Res.* **1988**, *21*, 387–394. [CrossRef]
14. Brestensky, D.M.; Stryker, J.M. Regioselective conjugate reduction and reductive silylation of α, β-unsaturated. *Tetrahedron Lett.* **1989**, *30*, 5677–5680. [CrossRef]
15. Miller, K.M.; Luanphaisarnnont, T.; Molinaro, C.; Jamison, T.F. Alkene-directed, nickel-catalyzed alkyne coupling reactions. *J. Am. Chem. Soc.* **2004**, *126*, 4130–4131. [CrossRef]
16. Brayshaw, S.K.; Harrison, A.; McIndoe, J.S.; Marken, F.; Raithby, P.R.; Warren, J.E.; Weller, A.S. Sequential reduction of high hydride count octahedral rhodium clusters $[Rh_6(PR_3)_6H_{12}][BArF_4]_2$: Redox-switchable hydrogen storage. *J. Am. Chem. Soc.* **2007**, *129*, 1793–1804. [CrossRef]
17. Shimizu, K.I.; Sato, R.; Satsuma, A. Direct C-C Cross-Coupling of Secondary and Primary Alcohols Catalyzed by a γ-Alumina-Supported Silver Subnanocluster. *Angew. Chem. Int. Ed.* **2009**, *48*, 3982–3986. [CrossRef]
18. Shimizu, K.I.; Sugino, K.; Sawabe, K.; Satsuma, A. Oxidant-Free Dehydrogenation of Alcohols Heterogeneously Catalyzed by Cooperation of Silver Clusters and Acid–Base Sites on Alumina. *Chem. Eur. J.* **2009**, *15*, 2341–2351. [CrossRef]
19. Shimizu, K.; Nishimura, M.; Satsuma, A. γ-Alumina-Supported Silver Cluster for N-Benzylation of Anilines with Alcohols. *ChemCatChem* **2009**, *1*, 497–503. [CrossRef]
20. Shimizu, K.-I.; Satsuma, A. Selective catalytic reduction of NO over supported silver catalysts—practical and mechanistic aspects. *Phys. Chem. Chem. Phys.* **2006**, *8*, 2677–2695. [CrossRef]
21. Shimizu, K.-I.; Satsuma, A. Reaction mechanism of H2-promoted selective catalytic reduction of NO with NH_3 over Ag/Al_2O_3. *J. Phys. Chem. C* **2007**, *111*, 2259–2264. [CrossRef]
22. Shimizu, K.-I.; Tsuzuki, M.; Kato, K.; Yokota, S.; Okumura, K.; Satsuma, A. Reductive activation of O_2 with H_2-reduced silver clusters as a key step in the H2-promoted selective catalytic reduction of NO with C_3H_8 over Ag/Al_2O_3. *J. Phys. Chem. C* **2007**, *111*, 950–959. [CrossRef]
23. Liao, J.H.; Dhayal, R.S.; Wang, X.; Kahlal, S.; Saillard, J.Y.; Liu, C.W. Neutron diffraction studies of a four-coordinated hydride in near square-planar geometry. *Inorg. Chem.* **2014**, *53*, 11140–11145. [CrossRef] [PubMed]
24. Dhayal, R.S.; Liao, J.H.; Lin, Y.R.; Liao, P.K.; Kahlal, S.; Saillard, J.Y.; Liu, C.W. A nanospheric polyhydrido copper cluster of elongated triangular orthobicupola array: Liberation of H_2 from solar energy. *J. Am. Chem. Soc.* **2013**, *135*, 4704–4707. [CrossRef] [PubMed]
25. Edwards, A.J.; Dhayal, R.S.; Liao, P.K.; Liao, J.H.; Chiang, M.H.; Piltz, R.O.; Kahlal, S.; Saillard, J.Y.; Liu, C.W. Chinese puzzle molecule: A 15 hydride, 28 copper atom nanoball. *Angew. Chem. Int. Ed.* **2014**, *53*, 7214–7218. [CrossRef]
26. Dhayal, R.S.; Chen, H.-P.; Liao, J.-H.; van Zyl, W.E.; Liu, C.W. Synthesis, Structural Characterization, and H_2 Evolution Study of a Spheroid-Shape Hydride-Rich Copper Nanocluster. *ChemistrySelect* **2018**, *3*, 3603–3610. [CrossRef]
27. Dhayal, R.S.; Liao, J.H.; Kahlal, S.; Wang, X.; Liu, Y.C.W.; Chiang, M.H.; van Zyl, W.E.; Saillard, J.Y.; Liu, C.W. $[Cu_{32}(H)_{20}\{S_2P(O^iPr)_2\}_{12}]$: The Largest Number of Hydrides Recorded in a Molecular Nanocluster by Neutron Diffraction. *Eur. J. Chem.* **2015**, *21*, 8369–8374. [CrossRef]
28. Brown, S.S.; Salter, I.D.; Šik, V.; Colquhoun, I.J.; McFarlane, W.; Bates, P.A.; Hursthouse, M.B.; Murray, M. The heteronuclear cluster chemistry of the group 1B metals. Part 9. Stereochemical non-rigidity of the metal skeletons of cluster compounds in solution. ^{109}Ag-{1H}INEPT nuclear magnetic resonance studies on $[Ag_2Ru_4(\mu_3\text{-}H)_2\{\mu\text{-}Ph_2P(CH_2)_nPPh_2\}(CO)_{12}]$(n = 1, 2, or 4) and X-ray crystal structure of $[Ag_2Ru_4(\mu_3\text{-}H)_2(\mu\text{-}Ph_2PCH_2PPh_2)(CO)_{12}]$. *J. Chem. Soc. Dalton Trans.* **1988**, *8*, 2177–2185. [CrossRef]
29. Beringhelli, T.; D'Alfonso, G.; Garavaglia, M.G.; Panigati, M.; Mercandelli, P.; Sironi, A. Synthesis, Solid-State Structure and Solution Behavior of Hydrido-Bridged Adducts between the Group 11 $[M(PPh_3)]^+$ Cations and the Triangular Cluster Anion $[Re_3(\mu\text{-}H)_4(CO)_9(PPh_3)]$. *Organometallics* **2002**, *21*, 2705–2714. [CrossRef]
30. Carreno, R.; Riera, V.; Ruiz, M.A.; Tiripicchio, A.; Tiripicchio-Camellini, M. Reactivity of $[Mn_2(.mu\text{-}H)_2(CO)_6$ (.mu.-tedip)](tedip=$(EtO)_2POP(OEt)_2$) with Group 11 Alkynyl Compounds. X-ray Structures of $[Ag_2Mn_4$ (.mu.-H)$_6(CO)_{12}$(.mu-tedip)$_2]$ and $[AuMn_4$(.mu.-H)$_5(CO)_{12}$(.mu-tedip)$_2]$. *Organometallics* **1994**, *13*, 993–1004. [CrossRef]
31. Gorol, M.; Mösch-Zanetti, N.C.; Roesky, H.W.; Noltemeyer, M.; Schmidt, H.-G. Unprecedented stabilisation of the Ag_2^{2+}-ion by two hydrido-iridium (iii) complexes. *Chem. Commun.* **2003**, 46–47. [CrossRef]
32. Albinati, A.; Chaloupka, S.; Demartin, F.; Koetzle, T.F.; Ruegger, H.; Venanzi, L.M.; Wolfer, M.K. Complexes with platinum-hydrogen-silver bonds. *J. Am. Chem. Soc.* **1993**, *115*, 169–175. [CrossRef]

33. Cook, A.W.; Nguyen, T.-A.D.; Buratto, W.R.; Wu, G.; Hayton, T.W. Synthesis, characterization, and reactivity of the group 11 hydrido clusters $[Ag_6H_4(dppm)_4(OAc)_2]$ and $[Cu_3H(dppm)_3(OAc)_2]$. *Inorg. Chem.* **2016**, *55*, 12435–12440. [CrossRef] [PubMed]
34. Liu, C.W.; Lin, Y.R.; Fang, C.S.; Latouche, C.; Kahlal, S.; Saillard, J.Y. $[Ag_7(H)\{E_2P(OR)_2\}_6]$ (E = Se, S): Precursors for the fabrication of silver nanoparticles. *Inorg. Chem.* **2013**, *52*, 2070–2077. [CrossRef] [PubMed]
35. Shi, W.; Ahlrichs, R.; Anson, C.E.; Rothenberger, A.; Schrodt, C.; Shafaei-Fallah, M. Reactions of P/S-containing proligands with coinage metal salts: A new route to polynuclear complexes with unusual structural types. *Chem. Commun.* **2005**, *47*, 5893–5895. [CrossRef]
36. Van Zyl, W.E. Dithiophosphonates and related P/S-type ligands of group 11 metals. *Comments Inorg. Chem.* **2010**, *31*, 13–45. [CrossRef]
37. Pillay, M.N.; Omondi, B.; Staples, R.J.; Van Zyl, W.E. A hexanuclear gold(I) metallatriangle derived from a chiral dithiophosphate: Synthesis, structure, luminescence and oxidative bromination reactivity. *CrystEngComm* **2013**, *15*, 4417–4421. [CrossRef]
38. Lee, Y.C.; Lin, Y.R.; Liou, B.Y.; Liao, J.H.; Gusarova, N.K.; Trofimov, B.A.; Van Zyl, W.E.; Liu, C.W. Dinuclear gold(I) dithio- and diselenophosph(in)ate complexes forming mononuclear gold(III) oxidative addition complexes and reversible chemical reductive elimination products. *Dalton Trans.* **2014**, *43*, 663–670. [CrossRef]
39. Ajayi, T.J.; Pillay, M.N.; Van Zyl, W.E. Solvent-free mechanochemical synthesis of dithiophosphonic acids and corresponding nickel(II) complexes. *Phosphorus Sulf. Silicon Relat. Elem.* **2017**, *192*, 1205–1211. [CrossRef]
40. Aditya, T.; Pal, A.; Pal, T. Nitroarene reduction: A trusted model reaction to test nanoparticle catalysts. *Chem Commun.* **2015**, *51*, 9410–9431. [CrossRef]
41. Zhao, P.; Feng, X.; Huang, D.; Yang, G.; Astruc, D. Basic concepts and recent advances in nitrophenol reduction by gold-and other transition metal nanoparticles. *Coord. Chem. Rev.* **2015**, *287*, 114–136. [CrossRef]
42. Rajegaonkar, P.S.; Deshpande, B.A.; More, M.S.; Waghmare, S.S.; Sangawe, V.V.; Inamdar, A.; Shirsat, M.D.; Adhapure, N.N. Catalytic reduction of *p*-nitrophenol and methylene blue by microbiologically synthesized silver nanoparticles. *Mater. Sci. Eng. C* **2018**, *93*, 623–629. [CrossRef] [PubMed]
43. Ai, L.; Jiang, J. Catalytic reduction of 4-nitrophenol by silver nanoparticles stabilized on environmentally benign macroscopic biopolymer hydrogel. *Bioresour. Technol.* **2013**, *132*, 374–377. [CrossRef] [PubMed]
44. Li, J.; Kuang, D.; Feng, Y.; Zhang, F.; Xu, Z.; Liu, M. A graphene oxide-based electrochemical sensor for sensitive determination of 4-nitrophenol. *J. Hazard. Mater.* **2012**, *201*, 250–259. [CrossRef] [PubMed]
45. Dong, X.-Y.; Gao, Z.-W.; Yang, K.-F.; Zhang, W.-Q.; Xu, L.-W. Nanosilver as a new generation of silver catalysts in organic transformations for efficient synthesis of fine chemicals. *Catal. Sci. Technol.* **2015**, *5*, 2554–2574. [CrossRef]
46. Kästner, C.; Thünemann, A.F. Catalytic reduction of 4-nitrophenol using silver nanoparticles with adjustable activity. *Langmuir* **2016**, *32*, 7383–7391. [CrossRef]
47. Begum, R.; Farooqi, Z.H.; Ahmed, E.; Naseem, K.; Ashraf, S.; Sharif, A.; Rehan, R. Catalytic reduction of 4-nitrophenol using silver nanoparticles-engineered poly (N-isopropylacrylamide-co-acrylamide) hybrid microgels. *Appl. Organomet. Chem.* **2017**, *31*, e3563. [CrossRef]
48. Liao, P.-K.; Fang, C.-S.; Edwards, A.J.; Kahlal, S.; Saillard, J.-Y.; Liu, C.W. Hydrido copper clusters supported by dithiocarbamates: Oxidative hydride removal and neutron diffraction analysis of $[Cu_7(H)\{S_2C(aza\text{-}15\text{-}crown\text{-}5)\}_6]$. *Inorg. Chem.* **2012**, *51*, 6577–6591. [CrossRef]
49. Liu, C.W.; Chang, H.-W.; Sarkar, B.; Saillard, J.-Y.; Kahlal, S.; Wu, Y.-Y. Stable Silver(I) Hydride Complexes Supported by Diselenophosphate Ligands. *Inorg. Chem.* **2010**, *49*, 468–475. [CrossRef]
50. Latouche, C.; Kahlal, S.; Lin, Y.-R.; Liao, J.-H.; Furet, E.; Liu, C.W.; Saillard, J.-Y. Anion encapsulation and geometric changes in hepta-and hexanuclear copper (I) dichalcogeno clusters: A theoretical and experimental investigation. *Inorg. Chem.* **2013**, *52*, 13253–13262. [CrossRef]
51. Xie, Y.; Yan, B.; Xu, H.; Chen, J.; Liu, Q.; Deng, Y.; Zeng, H. Highly Regenerable Mussel-Inspired Fe_3O_4@Polydopamine-Ag Core–Shell Microspheres as Catalyst and Adsorbent for Methylene Blue Removal. *ACS Appl. Mater. Int.* **2014**, *6*, 8845–8852. [CrossRef]
52. Baruah, B.; Gabriel, G.J.; Akbashev, M.J.; Booher, M.E. Facile synthesis of silver nanoparticles stabilized by cationic polynorbornenes and their catalytic activity in 4-nitrophenol reduction. *Langmuir* **2013**, *29*, 4225–4234. [CrossRef] [PubMed]
53. Kubas, G.J.; Monzyk, B.; Crumblis, A.L. Tetrakis(Acetonitrile)Copper(1+) Hexafluorophosphate(1-). *Inorg. Synth.* **1990**, *51*, 68–70. [CrossRef]
54. Van Zyl, W.E.; Woollins, J.D. The coordination chemistry of dithiophosphonates: An emerging and versatile ligand class. *Coord. Chem. Rev.* **2013**, *257*, 718–731. [CrossRef]
55. Yusuf, T.L.; Quadri, T.W.; Tolufashe, G.F.; Olasunkanmi, L.O.; Ebenso, E.E.; Van Zyl, W.E. Synthesis and structures of divalent Co, Ni, Zn and Cd complexes of mixed dichalcogen and dipnictogen ligands with corrosion inhibition properties: Experimental and computational studies. *RSC Adv.* **2020**, *10*, 41967–41982. [CrossRef] [PubMed]
56. Dolomanov, O.V.; Bourhis, L.J.; Gildea, R.J.; Howard, J.A.; Puschmann, H. OLEX2: A complete structure solution, refinement and analysis program. *J. Appl. Crystallogr.* **2009**, *42*, 339–341. [CrossRef]
57. Sheldrick, G. A short history of SHELX. *Acta Crystallogr. A* **2008**, *64*, 112–122. [CrossRef]
58. Sheldrick, G.A. Crystal structure refinement with SHELXL. *Acta Cryst. C* **2015**, *71*, 3–8. [CrossRef]